Journal of Alloys and Compounds 527 (2012) 40–47

Contents lists available at SciVerse ScienceDirect

Journal of Alloys and Compounds

journal homepage: www.elsevier.com/locate/jallcom

Detailed investigation of submicrometer-sized grains of chemically sprayed ($Sn_{1-x}Al_x$, O_2) ($0 \leq x \leq 0.085$) thin films

M. Benhaliliba[a,*], C.E. Benouis[a,**], F. Yakuphanoglu[b], A. Tiburcio-Silver[c], C. Aydin[b], S. Hamzaoui[d], Z. Mouffak[e]

[a] Physics Department, Science Faculty, Oran University of Sciences and Technology, USTOMB, BP1505 Oran, Algeria
[b] Firat University, Physics Department, Faculty of Sciences and Arts, 23119 Elazig, Turkey
[c] ITT-DIEE, Apdo, Postal 20, Metepec 3, 52176 Estado de Mexico, Mexico
[d] Laboratoire de Microscope Electronique et Sciences des Matériaux, USTOMB, BP1505 Oran, Algeria
[e] Department of Electrical and Computer Engineering, California State University, Fresno, CA, USA

ARTICLE INFO

Article history:
Received 9 February 2011
Received in revised form 18 February 2012
Accepted 24 February 2012
Available online xxx

Keywords:
Tin oxide
Spray pyrolysis
Al doping
Physical properties
Submicrometer structure
AFM

ABSTRACT

In this study, the submicrometer-sized grains of chemically sprayed tin oxide, SnO_2, were largely investigated. The films ($Sn_{1-x}O_2$, Al_x), with x = 0–0.085 were grown by spray pyrolysis onto glass at a fixed temperature of 300 °C. Structural, optical, electrical and morphological properties were studied. These films are polycrystalline in nature with a tetragonal crystalline structure, and exhibited a preferred orientation along the (2 0 0) planes. Atomic force microscope (AFM) analysis demonstrated a nano-grain structure. Our nanostructured films revealed high transparency in the visible and infra-red spectra and an electrical resistivity that ranged from 1 to1000 Ω cm.

1. Introduction

Tin oxide (SnO_2) has recently become one of the most studied materials in technology research, due to its various properties such as high transparency in visible range, high reflectivity in the infrared [1], direct band gap around 3.5 eV, and high exciton binding energy at room temperature (130 meV) [2]. It is well known that SnO_2 is a semiconductor that crystallizes in a tetragonal rutile structure [3]. SnO_2 films were grown by various processes like chemical precipitation route [4], chemical vapor deposition (CVD) [5], sputtering [6,7], sol–gel [8], pulsed laser deposition (PLD) [9], and spray pyrolysis deposition (SPD) [2,10,11]. This latter is a chemical deposition technique in which fine droplets of a solution containing desired species are sprayed on a preheated substrate. SPD is a facile technique that is low cost and permits easy doping [12]. With SPD, large and uniform SnO_2 films can be deposited at low temperature. This technique consists in a thermal decomposition that occurs on the hot substrate, giving rise to a continuous film as reported in literature [13]. SnO_2 is extensively used for a variety of applications including architectural windows, flat panel displays, smart windows, and film photovoltaic and polymer-based electronics [14]. Elements such as F, Cl, Sb, Br, Ni, Cu, Fe [12], Al [1], Co [15], and In [2], have been used as dopants for SnO_2. Tin oxide was grown on different substrates such as indium tin oxide (ITO) and silicon [16,17]. In this paper, we report on submicrometer-sized grains of ($Sn_{1-x}Al_x$, O_2) thin films chemically sprayed with different Al contents in the starting solution. Furthermore, we exhibit the characterizations and the role of Al concentration levels on chemically sprayed SnO_2 films properties.

2. Experimental procedures

2.1. Precursor preparation and deposition parameters

The deposition of the films was carried out by a homemade SPD technique, as sketched in Fig. 1. First, pure and Al-doped SnO_2 films were sprayed onto a corning glass 7059, near-zero alkali baria alumina borosilicate. The starting material was ($SnCl_4 \cdot 5H_2O$) and the doping source was aluminum (3+) chloride ($AlCl_3$). Both precursor and doping compounds were dissolved in methanol. The starting material concentration was 0.2 M and the concentration of the dopants Al/Sn in the solution were 1, 1.5, 3 and 8.5%. Spray rate and substrate to nozzle distance were maintained respectively at 20 ml/min and 25 cm. The glass substrate was heated at 300 °C which was controlled by a digital thermometer connected to the heater. Finally, the film thicknesses ranged between 150 and 270 nm.

* Corresponding author. Tel.: +213 41429212.
** Corresponding author. Tel.: +213 772211491; fax: +213 41424931.
E-mail addresses: mbenhaliliba@gmail.com, bmost_31@yahoo.fr (M. Benhaliliba), babimo14@yahoo.fr (C.E. Benouis).

0925-8388/$ – see front matter © 2012 Elsevier B.V. All rights reserved.
doi:10.1016/j.jallcom.2012.02.128

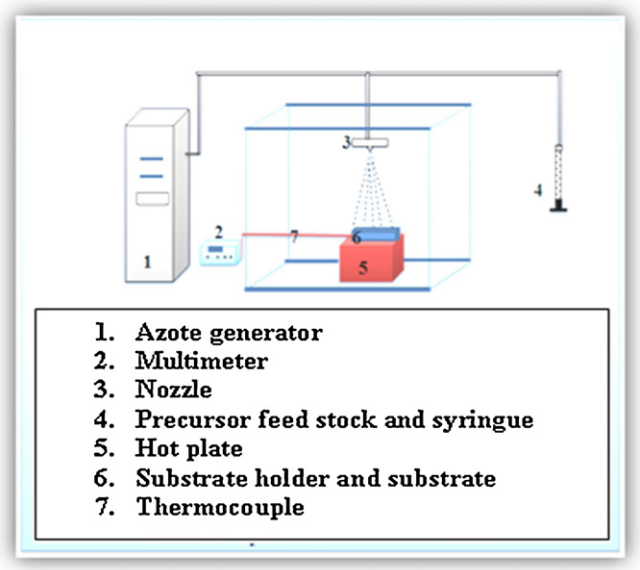

Fig. 1. Schematic diagram of spray pyrolysis deposition set-up.

2.2. Films characterization

X-rays diffraction patterns of the SnO_2 films were analyzed at room temperature using a Rigaku X-ray diffractometer, model DMAX 2200, having a copper anticathode (Cu Kα, 1.54 Å). The Bragg angle (2θ) ranged from 30° to 70°. The UV–VIS-NIR transmittance spectra of the SnO_2 films prepared at different concentrations of Al were recorded via a Shimadzu UV-3600 PC double beam spectrometer. The electrical resistivity measurement of the films was carried out by a Keithley 6517A electrometer at room temperature by two metal probes put in contact with the film, having a radius of 0.5 mm each and separated by 3–4 mm. The samples' morphology was investigated using a Park system XE-100 E atomic force microscope. Data measurements were taken at room temperature. Scans were made over areas ranging from 5 μm × 5 μm to 1 μm × 1 μm, and the scan rate ranged from 0.25 to 0.50 Hz. All AFM measurements described here were achieved with taping mode, non-contact silicon cantilever. AFM parameters details, such as section analysis, grain size distribution histogram, power spectral density (PSD) were deduced from XEI version 1.7.1 data processing and analysis software.

3. Results and discussion

3.1. Crystalline structure by XRD pattern analysis

The X-rays pattern spectra of pure and Al-doped SnO_2 were displayed in Fig. 2A. The as-grown films were identified as polycrystalline SnO_2 with a tetragonal crystal structure and preferred orientation along the (2 0 0) plane. Ours samples only exhibited the SnO_2 structure and no other was detected, as reported in the JCPDS card (No. 72-1147) data of SnO_2. Pure SnO_2 films revealed intense peak at $2\theta \sim 37.8°$ (see Fig. 2B). The main strong peaks were (2 0 0), (2 1 1) and (1 0 1) as evidenced in Fig. 2A which identifies the tetragonal structure (closed squares); the weak peaks (closed circles) demonstrated the presence of SnO_2 orthorhombic structure.

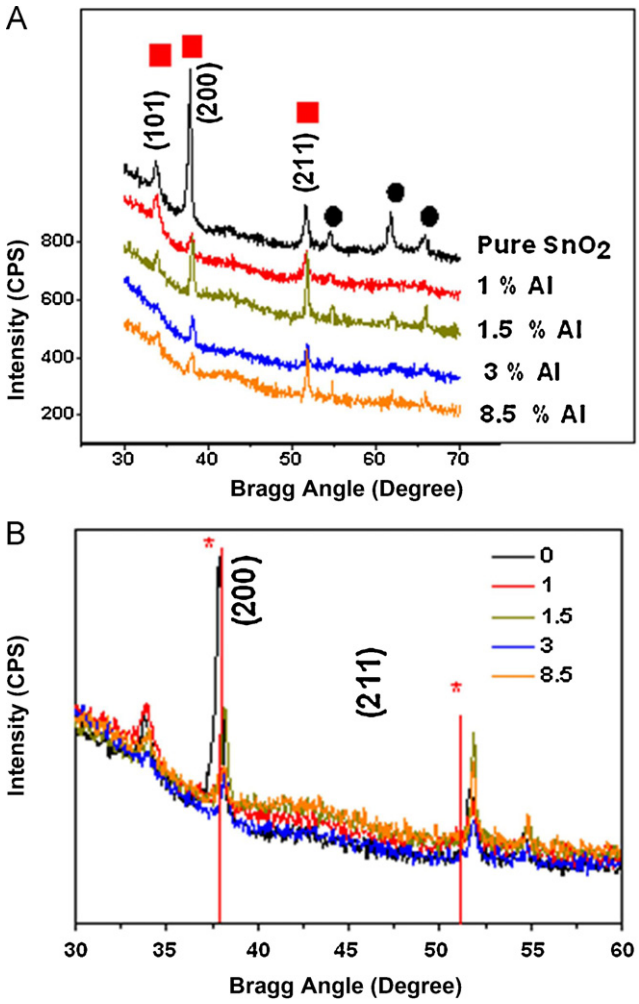

Fig. 2. (A) X-rays patterns of pure and Al doped SnO_2 grown by SPD: pure, 1%, 1.5%, 3% and 8.5% Al doped SnO_2. Peaks of SnO_2: red closed squares show tetragonal phase, while closed black circles show orthorhombic phase. (B) (2 0 0) and (2 1 1) orientations of pure and Al doped SnO_2 are evidenced, red lines of JCPDS 72-1147 card were signed by star. (For interpretation of the references to color in this figure legend, the reader is referred to the web version of this article.)

The peak (2 0 0) was very intense in the case of pure SnO_2, while Al doping levels reduced it. On the other hand, the (2 1 1) orientation of the films became more pronounced with Al content; mainly for doping levels of 1.5% and 8.5% sprayed films. Furthermore, the (1 0 1) direction diminished with the increase of Al content, whereas the peaks of orthorhombic SnO_2 became insignificant in the doped samples. Overall, these peaks presented a slight broadening (FWMH increases) which led us to report on nanostructures formation. This statement was confirmed by the small grain sizes of our samples (see Table 1). The increase of Al content led to a decrease in crystalline structure of the films, a result that was

Table 1
Structural (grain size according to (2 0 0) plane, lattice parameters a, Δa, c, Δc, ε_{zz}, V, $\Delta V/V$), optical (T at 550 nm), morphological (RMS, grain size by AFM analysis) parameters of pure and Al doped tin oxide.

Al level (%)	Grain size (XRD)(nm)	Lattice constants (Å)				ε_{zz} (%)	V (Å^3)	$\Delta V/V$ (%)	T (550 nm)	RMS (nm)	Grain size (AFM) (nm)
		A	Δa	c	Δc						
0	20.98	4.745	0.008	3.201	0.016	0.502	72.104	90.28	88.252	10.41	90.28
1	26.81	4.718	−0.019	3.218	0.033	1.036	71.660	149.31	75.475	19.09	149.31
1.5	21.61	4.712	−0.024	3.212	0.027	0.848	71.342	41.67	80.701	15.82	41.67
3	19.83	4.707	−0.030	3.219	0.034	1.067	71.343	27.78	77.439	10.84	27.78
8.5	21.57	4.715	−0.022	3.211	0.026	0.816	71.394	101.56	77.435	11.52	101.56

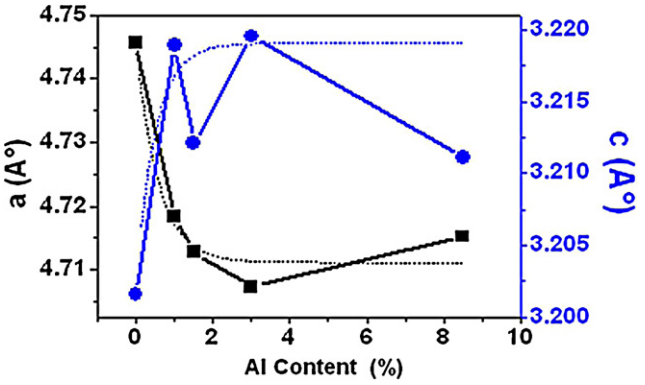

Fig. 3. Lattice parameters a and c of sprayed SnO_2 films were plotted versus Al content. Parameter a was fitted as exponential decay profile (black dash curve), and parameter c was fitted as SWeibull2 model (blue dash curve). (For interpretation of the references to color in this figure legend, the reader is referred to the web version of this article.)

also noticed by Ahmed et al. [18]. Similar crystalline structure and peak identification were reported in literature for Al-doped SnO_2 [13,15,18,19]. Amlouk reported the same trend for SnO2 thin layers, prepared at 440 °C [20]. (1 1 0), (1 0 1) and (2 1 1) are the preferential orientations in the case of Al-doped SnO2 films produced by sol gel dip coating as cited in literature [18,19]. Similar orientations were observed for the pure SnO_2 nanoparticles prepared by laser ablation [21]. Goyal et al. reported that (1 1 0), (2 0 0) and (2 1 1) were the main intense peaks in the case of Sb-doped SnO_2 grown by spray pyrolysis deposition [22]. A slight angle (2θ) shift was detected for the (2 0 0) direction, to the lower angle (pure sample) and to higher angle (Al-doped samples) as seen in Fig. 2B. This angle shift was also discussed by Lei for the Al-doped films [23]. In our study, for the selected scanned range of angle 2θ, the (1 0 1) direction was obviously seen in 0, 1 and 1.5% Al doped samples spectra, whereas it was less visible in 3 and 8.5% cases. The (2 0 0) orientation has been found to be strong for the pure tin oxide film; this peak intensity was reduced with increasing the aluminum doping levels. The (2 1 1) orientation was improved by the Al dopant in most of the samples. Fig. 3 depicted the variation of lattice parameters (a) and (c) versus Al doping levels. The lattice parameters a and c were determined from the expression 1 according to (2 0 0) direction [24],

$$\frac{1}{d_{hkl}} = \sqrt{\frac{h^2+k^2}{a^2} + \frac{l^2}{c^2}} \quad (1)$$

The values of lattice parameters a and c, unit cell volume V (Å^3), the differences $\Delta a = a - a_0$, $\Delta c = c - c_0$ (JCPDS-72-1147: $a_0 = b_0 = 4.737$ Å, $c_0 = 3.185$ Å), and the cell volume growth $\Delta V/V$ (%) were then listed in Table 1. We noticed that the lattice parameters a and c changed with Al doping levels, and the unit cell was then modified. The results were consistent with the improvement of the grain size and shape of the films depicted in the AFM picture. We observed that the unit cell was reduced according to (a) orientation and extended according to (c) orientation, a phenomenon certainly due to Al ion insertion into the SnO_2 lattice, whereas the pure sample showed an increase of both a and c directions. The Sn (+4) and Al (3+) ionic radii were respectively given, $r_{Sn} = 0.69$ Å and $r_{Al} = 0.54$ Å, and their ratio was $r_{Al(3+)}/r_{Sn(4+)} = 0.78$. Lei also reported that lattice constants of SnO_2 were expanded by Al doping [23]. Since the Al ion radius was lesser than tin ion radius which allowed an easy diffusion of the dopant atoms in the lattice of SnO_2, until the minimal energy of Al ions was reached. Knowing that a was fitted as exponential decay profile $a = Ae^{-x/t} + a_0$, where the following constants were, $A = 0.0345 \pm 0.005$, $t = 0.578 \pm 0.261$, $a_0 = 4.711 \pm 0.003$,

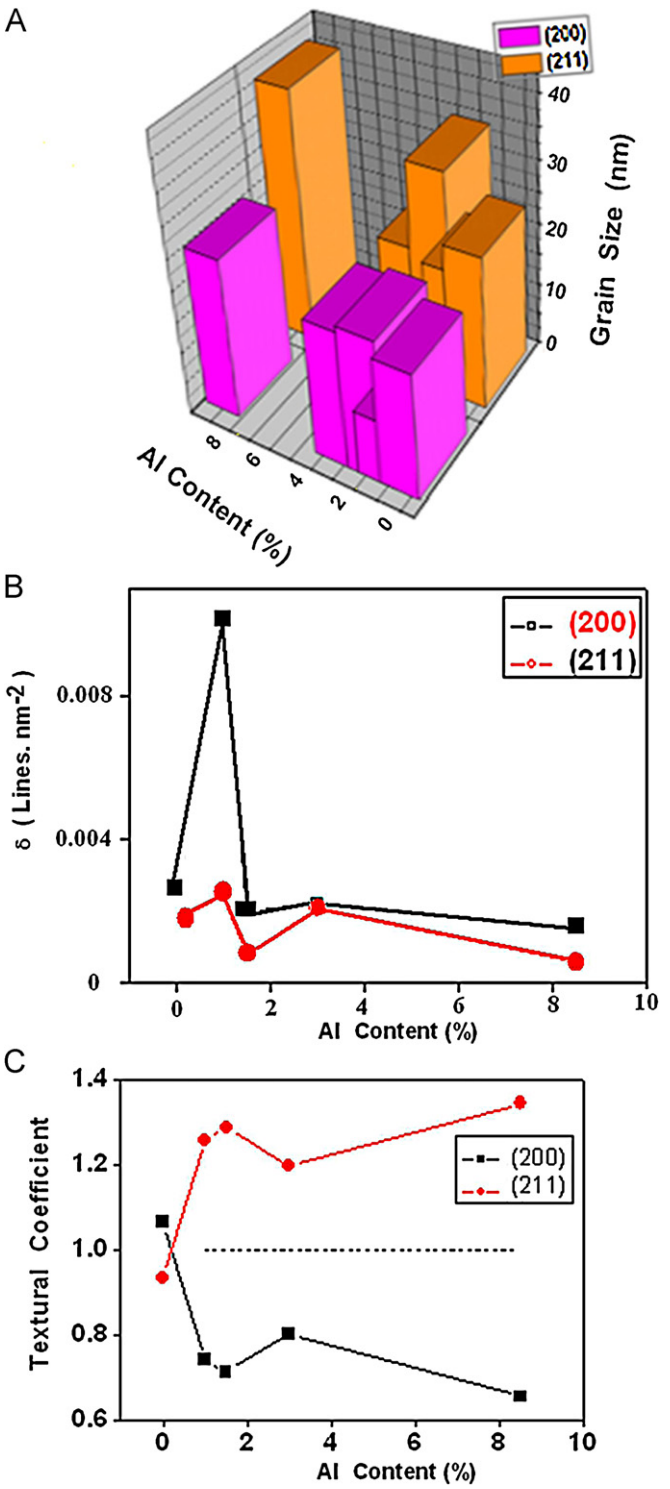

Fig. 4. (A) Dependence of grain size of sprayed SnO_2 films on Al content according to (2 0 0) and (2 1 1) orientations. (B) Variation of the dislocation density δ (lines nm^{-2}) of sprayed SnO_2 films with Al content according to (2 0 0) and (2 1 1) orientations. (C) Plot of textural coefficient of sprayed SnO_2 films with Al content according to (2 0 0) and (2 1 1) orientations. Average curve was sketched (black dash line).

and the parameter c was fitted as model $c = c_0 - (c_0 - \eta)e(-(kx)^d)$ where the constants were, $c_0 = 3.219$, $\eta = 3.201$, $k = 2$, $d = 1$. Fitted values of a were: 0% Al (4.746), 1% Al (4.717), 1.5% Al (4.713), 3% Al (4.711) and 8.5% Al (4.711) Å (see Fig. 3). Furthermore, chlorine was drastically present in the starting material and the doping precursor described above, which were sprayed at low deposition

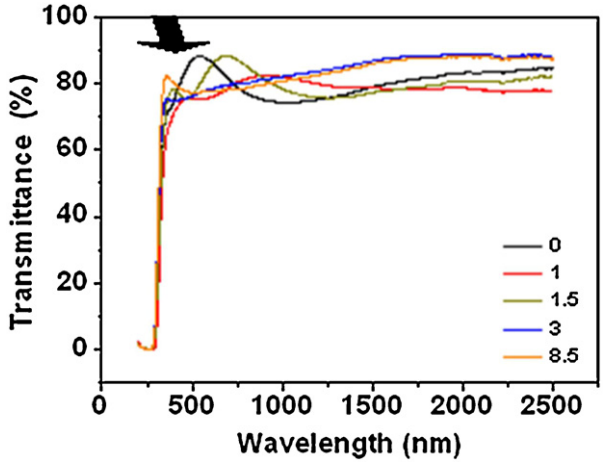

Fig. 5. Transmittance of pure and Al doped SnO_2 was plotted against photon wavelength. Arrow showed oscillations.

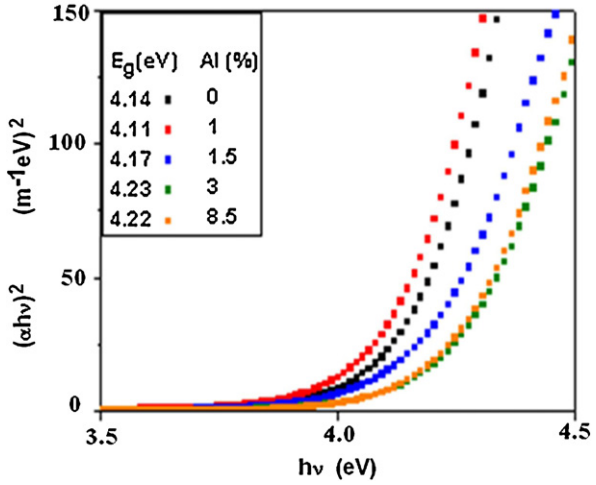

Fig. 6. Variations of $(\alpha h\nu)^2$ of sprayed SnO_2 films versus incident photon energy $h\nu$. Inset shows the obtained values of band gap energy E_g (eV).

temperature. The ionic radius of chlorine (Cl^-) 1.88 Å, being close to that of (O^{2-}) which is 1.40 Å; made it easy for chlorine ions to be incorporated into the SnO_2 lattice as substitutes to the oxygen ions. It seems that during the film growth, stacking faults, arising from the size difference between ions occur. In general, the proportion of carriers increases with the chlorine concentration in the film. Cl^- ions can substitute O^{2-} ions, which caused a number of electrons to become free. Ions of Cl^- were localized on certain sites and did not become donors, which led to a weak degree of crystalline structure without breaking the Sn—O bonds. The strain ε_{zz} along c orientation was expressed as [25],

$$\varepsilon_{zz} = \frac{(c - c_0)}{c_0} \times 100\% \quad (2)$$

where c is the lattice parameter of the strained SnO_2 films calculated from formula 1, and c_0 is unstrained lattice parameter, so the film became tensile if $\varepsilon_{zz} > 0$, or compressive, if $\varepsilon_{zz} < 0$, the obtained values of ε_{zz} were listed in Table 1. Consequently, we confirmed also that Al doping level improved the strain as can be seen in Table 1, and as we have mentioned before it was in well agreement with the lattice parameters change. Moreover the modified unit cell as a result of Al content was proved by parameter $\Delta V/V$ (%) as listed in Table 1. The film grain size G was given by Scherrer formula [26],

$$G = \frac{0.94\lambda}{\beta \cos\theta} \quad (3)$$

where λ is the wavelength of the X-ray used, β is the full width at half maximum which had maximum intensity and 2θ is the Bragg angle. Grain size according to (2 0 0) and (2 1 1) was plotted in Fig. 4A. According to (2 0 0) orientation, G varied from 19 nm to 27 nm (see Table 1). It has been found to vary from 13.5 nm to 43.8 nm according to (2 1 1) plane. The same grain size was found by Wei for spin coated Al:SnO_2 films [27]. The dislocation length per unit volume, was defined by the dislocation density δ (lines nm^{-2}), which measured the proportion of defects in a crystal as reported by Ravichandran [24]. The dislocation density was expressed as follows,

$$\delta = \frac{1}{G^2} \quad (4)$$

The evolution of δ was described in Fig. 4B according to (2 0 0) and (2 1 1) orientations. The higher values of δ ($\sim 10^{14}$ lines/m^2) were reached for 1% Al-doped SnO_2 when the lower dislocation density ($\sim 1.5\,10^{13}$ lines/m^2) was obtained for 8.5% Al-doped SnO_2 according to (2 0 0) direction. While the pure SnO_2 exhibited values of δ up to 2×10^{13} lines/m^2. These were of the same order of magnitude as those reported by Ravichandran [24]. Similar shape was observed according to (2 1 1) direction [27]. Therefore, the degree of crystallization (d_{cryst}) of pure and Al-doped SnO_2 was evidenced by the value of δ ($\delta \sim 1/d_{cryst}$) as displayed in Fig. 4B. We observed the same shape for both orientations. The variation of dislocation density depended on aluminum content. The texture coefficient expressed as $TC = I_{200}/[(I_{200} + I_{211} + I_{101})/3]$ [2] was sketched in Fig. 4C according to (2 0 0) and (2 1 1) orientations. The influence of Al doping on TC was extremely confirmed according to both (2 0 0) and (2 1 1) planes. In the (2 1 1) direction, TC increased with Al content while it decreased according to (2 0 0).

3.2. Optical characterization

The UV–VIS-NIR spectra of transmittance of pure and Al-doped tin oxide were depicted in Fig. 5. Pure samples revealed oscillations, similar trend was found by Senthilkumar for tin oxide prepared by electron beam evaporation technique [28], and by Wang for electrospun tin oxide nanofibers [29]. Furthermore, transmittance increased rapidly in the UV range and strong oscillations were observed in the VIS range for the 0, 1 and 1.5% Al-doped tin oxide samples. These oscillations might be due to the difference in film thickness. The oscillations were observed in 2.31, 12.05 and 18.56% Al-doped SnO_2 produced by sol gel technique as reported by Ahmed [18,19], and by Ravichandran in SnO_2–ZnO films [24]. Our samples exhibited significant fluctuations of the transmittance in VIS-IR

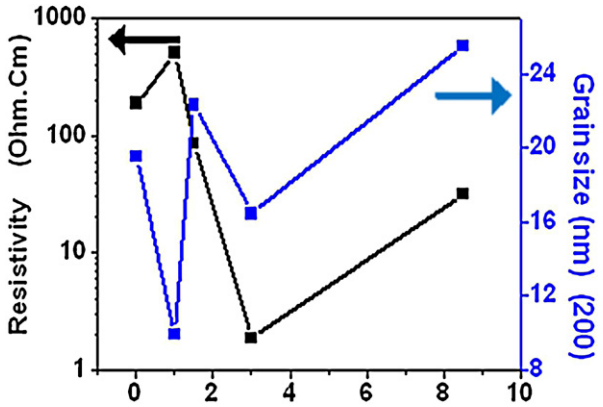

Fig. 7. Plot of electrical resistivity (semi-log scale) of sprayed SnO_2 films against Al content (left). Grain size versus Al content was plotted (right).

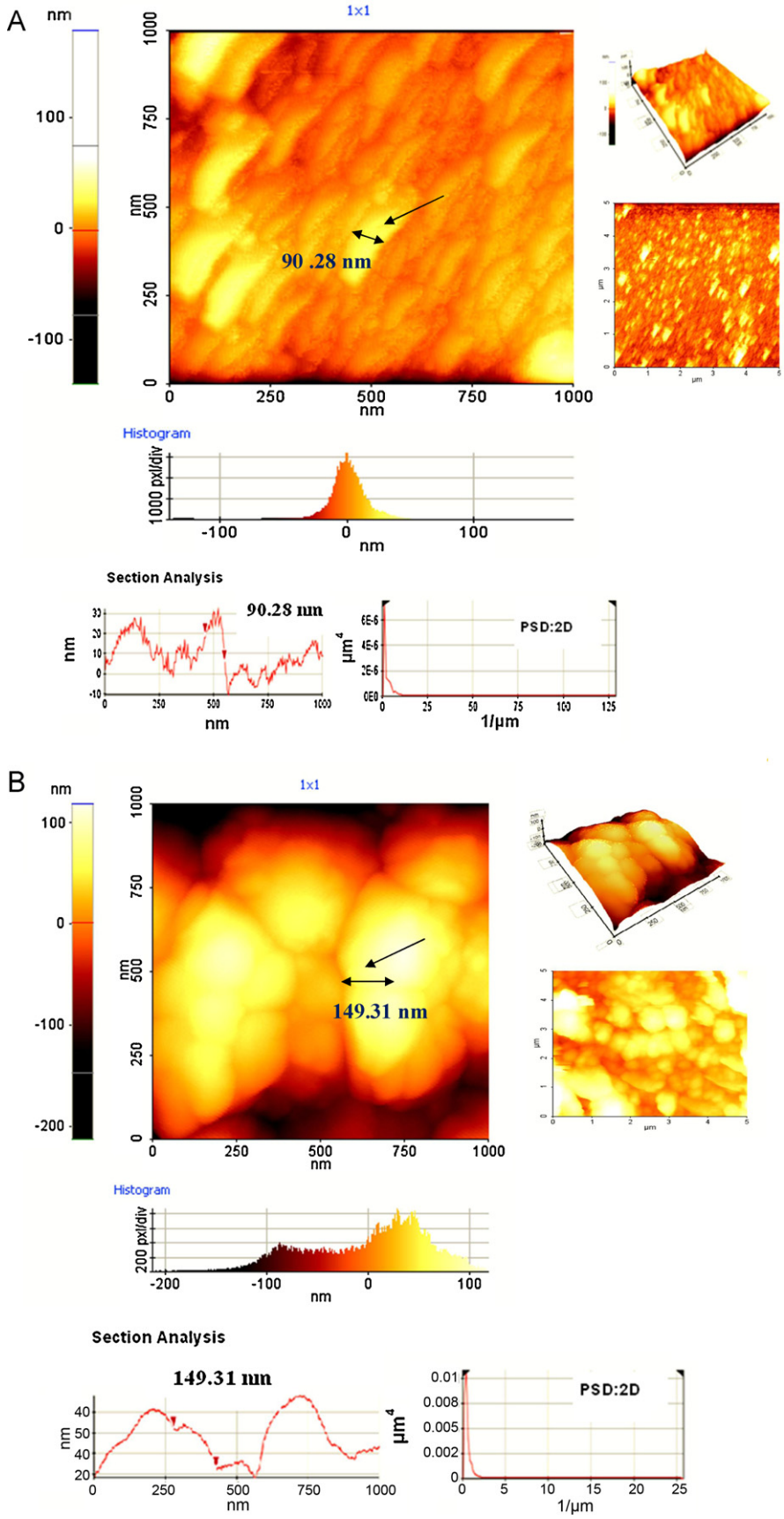

Fig. 8. Atomic force microscope (AFM) topography image of sprayed SnO_2 films at 300 °C (A: pure SnO_2, B: Al 1%, C: Al 1.5%, D: 3 Al% and E: 8.5 Al%): 2D view (1 μm × 1 μm) nanograins, nanorods were signed by black arrows. Grain size was marked by black arrow in 2D-image and by two red arrows in section analysis (left), 3D-view (right up) and 2D-view (5 μm × 5 μm) (right down), grain size distribution histograms, section analysis and power spectral density function (PSD) were displayed at bottom.

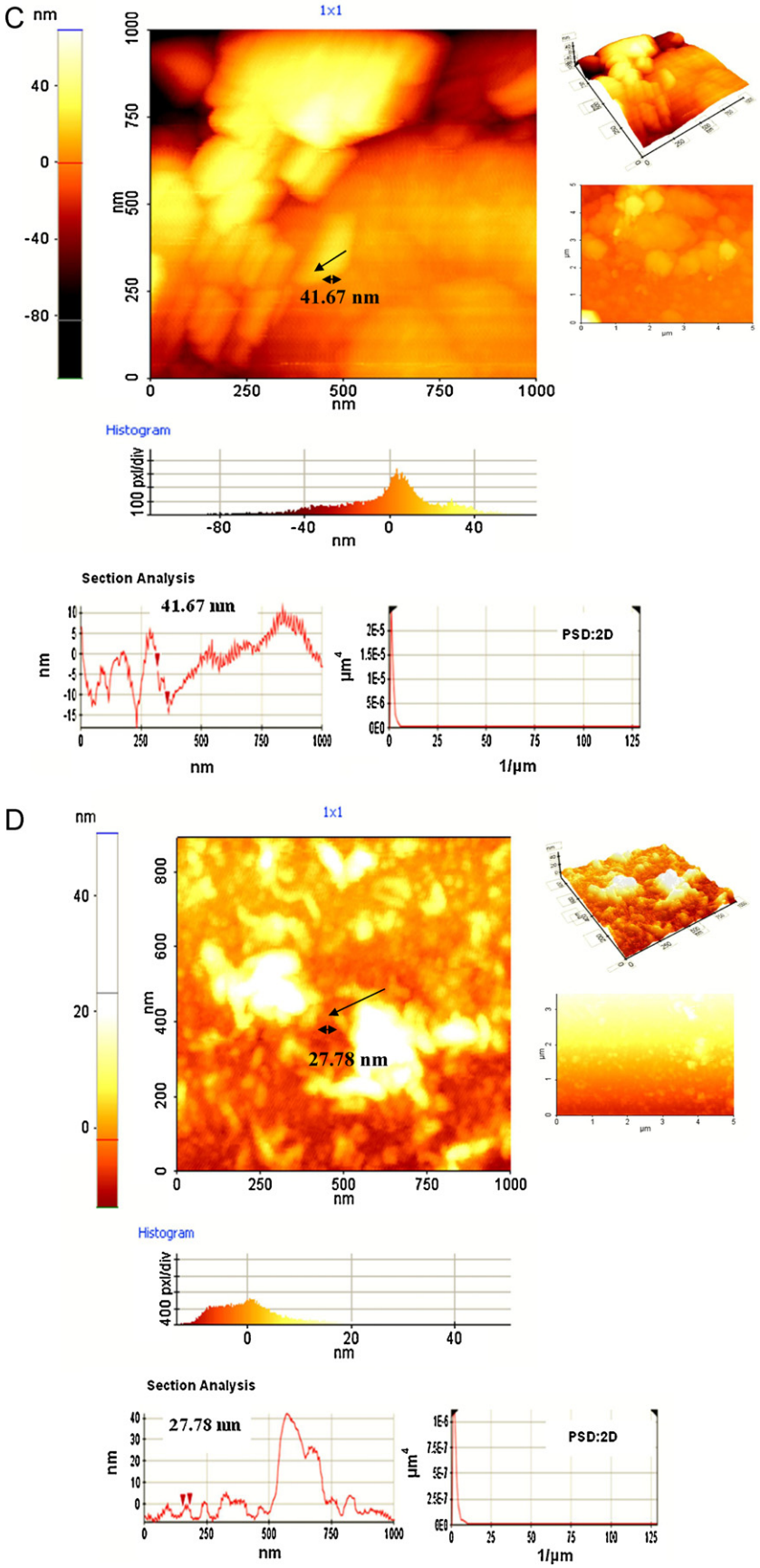

Fig. 8. (*Continued*)

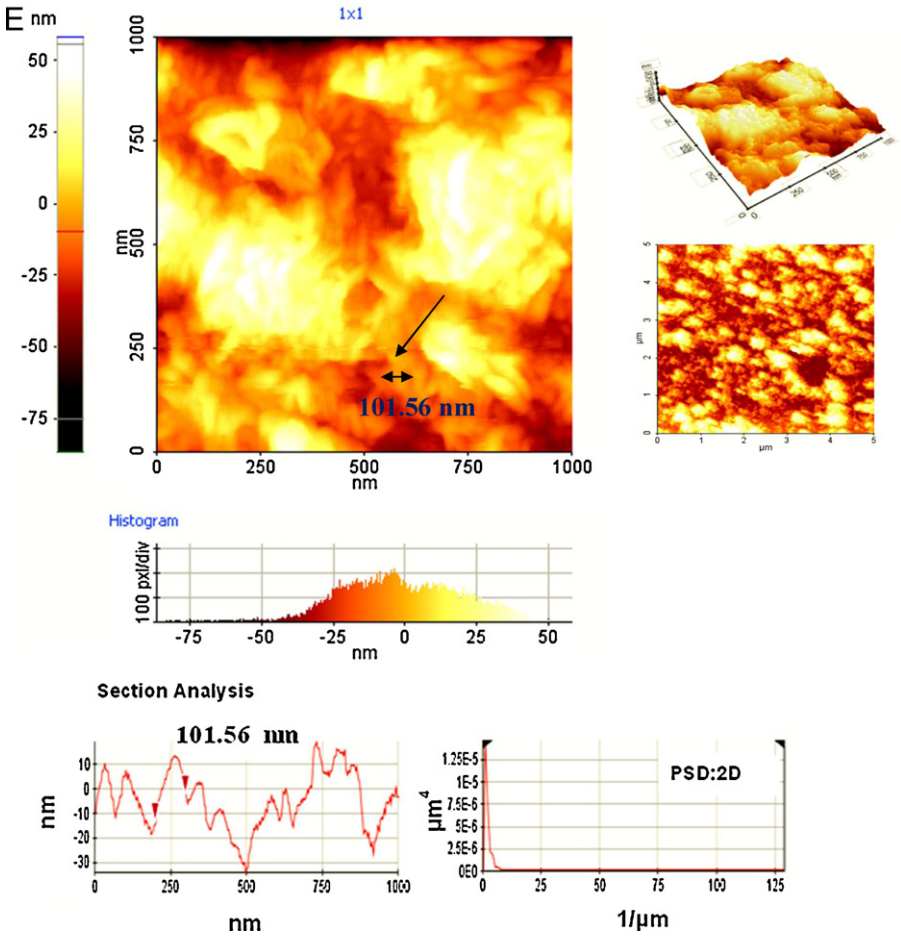

Fig. 8. (*Continued*).

spectrum around an average equal to 82%. Transmittance values at 550 nm were tabulated below. The same trend was found by Martinez, Lee and Seo [30–32]. Fig. 6 depicts the absorption coefficient $(\alpha h\nu)^2$ against incident photon energy $(h\nu)$. We can clearly see the Al content effect on the optical band gap. The band gap energy for allowed direct transitions was given by formula (5) [26],

$$\alpha h\nu = (h\nu - E_g)^{1/2} \tag{5}$$

where α is the absorption coefficient, h is Planck's constant, ν is the photon frequency, and E_g is the band gap energy. By extrapolation of the linear part of the curve, the intersection with energy axis determined the band gap E_g, which ranged from 4.11 to 4.24 eV, while the pure SnO_2 exhibited a band gap found to be 4.14 eV as can be easily seen in the inset of Fig. 6, consequently the discrepancy of E_g was due to Al doping levels. Our results were in accordance with those found by Bagheri Mohagheghi and Shokooh-Saremi ($3.60 < E_g < 4.20$) [33]. In addition, ions of Pt and Pd reduced the optical band gap from 4 eV to 2.8 eV [34]. Fluorine ions changed very slightly the optical band gap of SnO_2 [35]. SnO_2, prepared by sol gel route, exhibited an optical band gap of 3.48–3.72 eV [36] and iron ions reduced the value of E_g from 3.87 to 3.38 eV [37].

3.3. Electrical measurements

The electrical resistivity ρ of pure and Al-doped SnO_2 was shown in Fig. 7. The samples exhibited a resistivity range of 1–1000 Ω cm. The electrical resistance R (Ω) was given by expression (6), where ρ was the electrical resistivity of the film, l was the length between two metal contacts, and A was their area,

$$R = \rho\frac{l}{A} \tag{6}$$

At room temperature, the resistivity has been found to vary from 0.73 to 6.25 Ω cm as cited by Ahmed et al. [19]. Lower values of resistivity were reported in literature, for pure SnO_2 (2.71×10^{-2} Ω cm) and 2% Al-doped SnO_2 (6.7×10^{-2} Ω cm) and the resistivity increased with Al doping level [38]. High resistivity of pure SnO_2 (~10 KΩ cm) was obtained by Li [39]. Further, minor values of resistivity (172.37 and 704.25 Ω cm) were detected for the Sb-doped SnO_2 sample [40]. Our samples demonstrated a resistivity increase due to chlorine incorporation and the low substrate temperature as mentioned previously. In literature, similar films ($\rho \sim 2$ KΩ cm), were prepared by reactive sputtering [41]. The resistivity of samples depended on grain size as shown in Fig. 7. Resistivity of films was not reduced as much as it depends more on the density of charge carriers and their mobility.

3.4. AFM morphology observation

The nanostructure morphology of the SnO_2 films was analyzed by AFM. The grains sizes of our films ranged within 27–150 nm. We confirmed that both Al doping and its level had influence on grain structures as sketched in Fig. 8A–E. Nanograin-like assembled islands were shaped in the 1.5% Al-doped tin oxide film. These results were in good agreement with those found by Hamd et al. and large sized grains exceeding 100 nm were confirmed [42]. Kim

had found analogous shapes by AFM for pure SnO_2 grown by PLD technique [43]. Other researchers like Khandelwal reported that tin oxide exhibited columnar profile [44]. Overall, the surface was homogenous and grains have different sizes. Moreover the grains grown according to (2 0 0) preferential direction had well-defined boundaries, these results corroborated with those given by X-ray pattern. In summary, the pure tin oxide nanostructures looked like rods with an average radius found to be 90 nm (see Fig. 8A up-left). For the 1% Al-doped films, the grains looked like nano-islands with an average size found to be 150 nm, with no well-defined boundaries, which expanded the whole surface with few voids as seen in micrograph (Fig. 8B). The observed grains were clearly longer and seem to be nanorods which were pointed to by an arrow on the micrographs. The nanorods grew according to (2 0 0) orientation, furthermore the Al ions' presence made the nanorods thinner as the Al content increased (Al 1.5%). The nanorods of 3% Al-doped films became thinner and wavier with a size of 30 nm (see Fig. 8D). Finally, in the case of 8.5% Al, grains were assembled in clusters, and looked roughly like flowers, as can be seen in Fig. 8 D and E (2 and 3-dimensional views (2D) and (3D)). Zhao reported that SnO_2 flower-like architecture had been synthesized by hydrothermal technique [45]. The high roughness of surface was detected in 1% Al-doped SnO_2 films as listed in Table 1. The smooth surfaces were those of pure and 3% Al-doped SnO_2 (root mean square roughness (RMS) ~10 nm). It would generally be considered that the surface morphology of grown films was related to constituent element parameters such as surface thermal energy and mass diffusion [46]. The histogram distribution depicted the number of pixels per division; the section analysis and PSD of nano-films were described in Fig. 8 (bottom). The section analysis demonstrated the grain size by two red arrows, smaller SnO_2 nano-clusters was grown by thermal decomposition process (from 1.5 nm to 4 nm) as demonstrated by Salavati-Niasari [47].

4. Conclusions

In summary, nanostructures of sprayed aluminum-doped SnO_2 films were investigated. A careful study revealed that the Al doping level greatly influenced the structural, morphological, optical and electrical properties. These films were found to be polycrystalline with a tetragonal crystal structure, which grew according to the preferential (2 0 0) orientation with grain size of 19–27 nm. Lattice parameters, $a = 4.707–4.745$ Å, and $c = 3.201–3.219$ Å, were affected by the incorporation of Al in the unit cell of tin oxide. Additionally, the SnO_2 films were tensile ($0.5 < \varepsilon_{zz} < 1.1$) and cell volume growth $\Delta V/V$ (%) increased with Al content. The Al doping reduced the transmittance and high transparency of the film was demonstrated ($T_{average} \sim 83\%$). The optical band gap was found to be 4.14 eV for pure tin oxide and was modified by Al level doping. Film resistivity changed with grain size as a result of Al content. Grains, having a size range of 25–150 nm showed a nanorods' structure and became nano-flowers when Al rate exceeded 2%. The following characteristics, low resistivity, high transmittance (~77.5%), major crystalline structure TC (~0.8), a grain size of 25 nm, little surface roughness (10.8 nm), made 3% Al doped tin oxide the best candidate for many applications in micro-optoelectronic devices.

Acknowledgments

The work is included in the PNR project under contract number 8/U311/R77, supported by "agence nationale pour le développement de la recherche universitaire" (ANDRU) http://www.andru.gov.dz, and National Administration of Scientific Research (NASR) http://www.nasr-dz.org. It is a part of "*CNEPRU2009-2012*" supported by the Algerian High Level Teaching and Scientific Research Ministry MESRS and Oran Sciences and Technology University USTOMB. The authors gratefully acknowledge the generous assistance of Pr. M. Caglar for the X-rays analysis, Anadolu University Eskisehir, Turkey.

References

[1] J. Zhao, X.J. Zhao, J.M. Ni, H.Z. Tao, Acta Mater. 58 (2010) 6243–6248.
[2] C.E. Benouis, M. Benhaliliba, F. Yakuphanoglu, A. Tiburcio Silver, M.S. Aida, A. Sanchez Juarez, Synth. Met. 161 (2011) 1509–1516.
[3] W. Shuo, Z. Qingnan, M. Dengkui, D. Yuhong, J. Rare Earth 28 (2010) 189–193.
[4] J. Chen, J. Xu, Sens. Actuators B 157 (2011) 494–499.
[5] I. Volintiru, A. de Graaf, J. Van Deelen, P. Poodt, Thin Solid Films 519 (2011) 6258–6263.
[6] C. Körber, P. Ágoston, A. Klein, Sens. Actuators B 139 (2009) 665–672.
[7] Y. Muto, et al., Thin Solid Films (2011), doi:10.1016/j.tsf.2011.04.151.
[8] D.Y. Torres Martínez, R. Castanedo Pérez, G. Torres Delgado, O. Zelaya Angel, J. Mater. Sci. Mater. Electron. 22 (2011) 684–689.
[9] Z.W. Chen, Z. Jiao, M.H. Wu, C.H. Shek, C.M.L. Wu, J.K.L. Lai, Prog. Mater. Sci. 56 (2011) 901–1029.
[10] A.R. Babar, S.S. Shinde, A.V. Moholkar, C.H. Bhosale, J.H. Kim, K.Y. Rajpure, J. Alloys Compd. 509 (2011) 3108–3115.
[11] B. Zhang, Y. Tian, J.X. Zhang, W. Cai, Vacuum 85 (2011) 986–989.
[12] V. Bilgin, I. Akyuz, E. Ketenci, S. Kose, F. Atay, Appl. Surf. Sci. 256 (2010) 6586–6591.
[13] C. Thanachayanont, V. Yordsri, C. Boothroyd, Mater. Lett. 65 (2011) 2610–2613.
[14] B. Zhang, Y. Tian, J.X. Zhang, W. Cai, Mater. Lett. 65 (2011) 1204–1206.
[15] G. Korotcenkov, B.K. Cho, M. Nazarov, D.Y. Noh, E.V. Kolesnikova, Curr. Appl. Phys. 10 (2010) 1123–1131.
[16] M. Benhaliliba, C.E. Benouis, Y.S. Ocak and F. Yakuphanoglu, J. Nano-Electron. Phys. 4 (1), 01011 (2012) 3.
[17] J. Jeong, D.-S. Na, B.-J. Lee, H.-J. Song, H.-G. Kim, Curr. Appl. Phys. 12 (2012) 303–306.
[18] Sk.F. Ahmed, P.K. Ghosh, S. Khan, M.K. Mitra, K.K. Chattopadhyay, Appl. Phys. A 86 (2007) 139–143, doi:10.1007/s00339-006-3734-6.
[19] Sk.F. Ahmed, S. Khan, P.K. Ghosh, M.K. Mitra, K.K. Chattopadhyay, J. Sol–Gel Sci. Technol. 39 (2006) 241–247, doi:10.1007/s10971-006-7808-x.
[20] A. Amlouk, K. Boubaker, M. Amlouk, J. Alloys Compd. 490 (2010) 602–604.
[21] M.A. Gondal, Q.A. Drmosh, T.A. Saleh, Appl. Surf. Sci. 256 (2010) 7067–7070.
[22] D.J. Goyal, C. Agashe, M.G. Takwale, V.G. Bhide, J. Cryst. Growth 130 (1993) 567–570.
[23] M. Lei, Q.R. Hu, S.L. Wang, W.H. Tang, Mater. Lett. 64 (2010) 19–21.
[24] K. Ravichandran, B. Sakthivel, P. Philominathan, Cryst. Res. Technol. 45 (3) (2010) 292–298.
[25] X. Teng, H. Fan, S. Pan, C. Ye, G. Li, Mater. Lett. 61 (2007) 201–204.
[26] M. Benhaliliba, C.E. Benouis, M.S. Aida, F. Yakuphanoglu, A. Sanchez Juarez, J. Sol–Gel Sci. Technol. 55 (2010) 335–342.
[27] L. Wei, C. Lili, Sci. China (Ser. B) 44 (2001) 63–67.
[28] V. Senthilkumar, P. Vickraman, J. Mater. Sci. Mater. Electron. 21 (2010) 578–583, doi:10.1007/s10854-009-9960-x.
[29] Y. Wang, I. Ramos, J.J. Santiago-Aviles, J. Appl. Phys. 102 (2007) 093517.
[30] A.I. Martinez, D.R. Acosta, Thin Solid Films 483 (2005) 107–113.
[31] J. Lee, Thin Solid Films 516 (2008) 1386–1390.
[32] Y.J. Seo, G.W. Kim, C.H. Sung, M.S. Anwar, C.G. Lee, B.H. Koo, Curr. Appl. Phys. (2010), doi:10.1016/j.cap.2010.11.070.
[33] M.M. Bagheri Mohagheghi, M. Shokooh-Saremi, Physica B 405 (2010) 4205–4210.
[34] M. Gaidi, A. Hajjaji, M.A.E. Khakani, B. Chenevier, M. Labeau, B. Bessais, J. Appl. Phys. 48 (2009) 072501.
[35] F. Atay, V. Bilgin, I. Akyuz, E. Ketenci, S. Kose, J. Non-Cryst. Solids 356 (2010) 2192–2197.
[36] R. Lorenzi, et al., J. Non-Cryst. Solids (2011), doi:10.1016/j. jnoncrysol.2010.12.045.
[37] T.N. Soitah, et al., Mater. Sci. Semicond. Process. (2011), doi:10.1016/j.mssp.2010.03.002.
[38] M.M. Bagheri Mohagheghi, M. Shokooh Saremi, J. Phys. D: Appl. Phys. 37 (2004) 1248–1253.
[39] Y.Q. Li, J.-L. Wang, S.-Y. Fu, S.-G. Mei, J.-M. Zhang, K. Yong, Mater. Res. Bull. 45 (2010) 677–681.
[40] F. Bai, Y. He, P. He, Y. Tang, Z. Jia, Mater. Lett. 60 (2006) 3126–3129.
[41] A. Czapla, E. Kusior, M. Bucko, Thin Solid Films 182 (1989) 15–22.
[42] W. Hamd, Y.C. Wu, A. Boulle, E. Thune, R. Guinebretière, Thin Solid Films 518 (2009) 1–5.
[43] C.K. Kim, S.M. Choi, I.H. Noh, J.H. Lee, C. Hong, H.B. Chae, G.E. Jang, H.D. Park, Sens. Actuators B: Chem. 77 (2001) 463–467.
[44] R. Khandelwal, A.P. Singh, A. Kapoor, S. Grigorescu, P. Miglietta, N.E. Stankova, A. Perrone, Opt. Laser Technol. 41 (2009) 89–93.
[45] Q. Zhao, Z. Li, C. Wu, X. Bai, Y. Xie, J. Nanopart. Res. 8 (6) (2006) 1065–1069, doi:10.1007/s11051-006-9110-9.
[46] S. Chacko, N.S. Philip, K.G. Gopchandran, P. Koshy, V.K. Vaidyan, Appl. Surf. Sci. 254 (2008) 2179–2186.
[47] M. Salavati-Niasari, N. Mir, F. Davar, Inorg. Chim. Acta 363 (2010) 1719–1726.